ChemComm

Accepted Manuscript

This article can be cited before page numbers have been issued, to do this please use: L. Meng, Y. Li, R. Yang, X. Zhang, C. Du and J. Chen, *Chem. Commun.*, 2019, DOI: 10.1039/C8CC09411J.

ROYAL SOCIETY OF CHEMISTRY

rsc.li/chemcomm

ROYAL SOCIETY OF CHEMISTRY View Article Online
DOI: 10.1039/C8CC09411J

Journal Name

COMMUNICATION

Sensitive photoelectrochemical assay of miRNA-155 based on CdSe QDs//NPC-ZnO polyhedra photocurrent-direction switching system and target-triggered strand displacement amplification strategy

Received 00th January 20xx,
Accepted 00th January 20xx

DOI: 10.1039/x0xx00000x

www.rsc.org/

Leixia Meng, Yanmei Li, Ruiying Yang, Xiaohua Zhang*, Cuicui Du, Jinhua Chen *

Herein, a new photoelectrochemical (PEC) biosensor based on photocurrent direction switching system and target-triggered strand displacement amplification strategy has been developed for sensitive detection of microRNA (miRNA)-155, and shows excellent selectivity and a low detection limit of about 49 aM.

Photoelectrochemical (PEC) assay, as a germinating and promising analytical method, has received considerable interest due to its low background signal and good sensitivity.[1-4] Besides, the PEC technique has additional merits of simplicity, economy and miniaturization.[5-6] To improve the sensitivity of the PEC assay, a series of PEC sensors based on the steric-hindrance, energy transfer effect, biocatalytic precipitation and in-situ consumption/production of electron donor/acceptor have been developed in the past decades.[7-12] On the other hand, in order to improve the selectivity of the PEC method, the PEC sensing interface was usually blocked by some organic molecules or biomolecules, such as 6-mercaptohexanol (MCH), serum albumin (BSA) and peptides.[13-18] Recently, Yuan et al. developed a new PEC sensor with zero background based on the DNA tetrahedron and CdTe QDs-methylene blue probe.[19] These methods only amplify the PEC response currents or depress its background currents without the change of the photocurrent direction, can not avoid the possible false positive or negative signal due to the coexisting oxidative or reductive interferents and non-redox active biomolecules. In order to fundamentally avoid the false positive or negative signal, the target-induced switch of photocurrent direction may be a promising method for PEC sensors. However, only a few works addressed on this topic.[20,21] For example, Dai et al. developed an immunosensor for the detection of human interleukin-6 (IL-6) based on silver iodide (AgI) tags as a photocurrent direction converter of carbon nitride (CN).[20] However, the switched PEC response current was very small (nA) due to the large electrochemical impedance from the AgI-induced biocatalytic precipitation, which would be a burden on the assay sensitivity of the PEC sensors. Therefore, a new photocurrent-direction switching system with a large switched PEC response current is highly desired for sensitive PEC assay.

Owing to low cost and good photostability, CdSe quantum dots (QDs), n-type semiconductors, were used widely as the photoactive material to construct PEC biosensor.[22,23] On the other hand, our group recently developed a new PEC active material, nitrogen-doped porous carbon-ZnO polyhedra (NPC-ZnO) obtained via the carbonization treatment of zeolitic imidazolate framework (ZIF)-8, and found that NPC-ZnO was a p-type semiconductor and had excellent PEC behavior in visible light range.[15] These inspire us to construct a new photocurrent-direction switching system based on n-type CdSe QDs and p-type NPC-ZnO.

Here, taking microRNA (miRNA)-155 as a model due to its important roles as potential biomarker for early diagnosis and prediction of cancers,[24] a novel PEC biosensor has been developed based on the CdSe QDs//NPC-ZnO polyhedra photocurrent-direction switching system and target-triggered strand displacement amplification (SDA) strategy (Scheme 1). Before the modification of CdSe QDs on the indium tin oxide (ITO) electrode, the poly(diallyldimethylammonium chloride) (PDDA)-modified reduced graphene oxide (P-rGO) with positive charge was coated on the ITO electrode. P-rGO not only acted as an excellent electron transport matrix to improve the charge separation efficiency, but also as a carrier to effectively immobilize and disperse CdSe QDs. Hairpin DNA probe 1 (HP1) was then immobilized on the ITO electrode and opened in the presence of miRNA-155. After that, the biotinylated hairpin DNA probe 2 (HP2) hybridized with the exposed complementary sequence of HP1, resulting in the release of miRNA-155. The free miRNA-155 was available for the another hybridization event, which produced considerable

State Key Laboratory of Chemo/Biosensing and Chemometrics, College of Chemistry and Chemical Engineering, Hunan University, Changsha, 410082, P.R. China.
E-mail: chenjinhua@hnu.edu.cn, mickyxie@hnu.edu.cn; Fax: +86-731-88821848; Tel: +86-731-88821848.

†Electronic Supplementary Information (ESI) available: DNA and miRNA sequences used in this work; Experimental section; Material characterization; Cathodic and anodic linear potential scans; Optimization of experimental conditions; Recovery test. See DOI: 10.1039/x0xx00000x

View Article Online
DOI: 10.1039/C8CC09411J

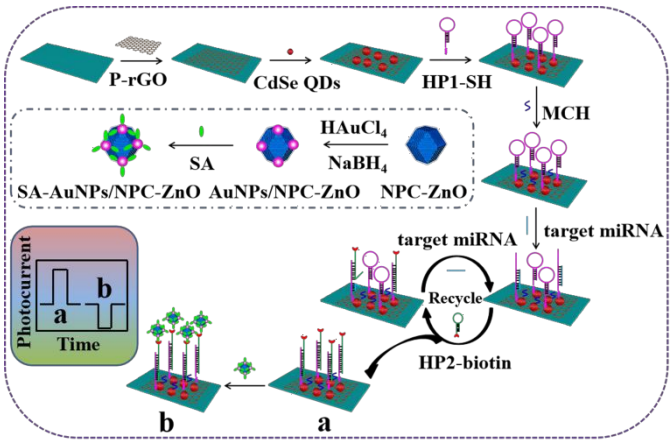

Scheme 1. Schematic diagram of the preparation of PEC biosensor for miRNA-155 detection based on photocurrent direction switching system and target-triggered strand displacement amplification strategy.

HP1-HP2 duplex on the electrode. Finally, the streptavidin (SA)-labeled AuNPs/NPC-ZnO polyhedra were attached to the electrode surface by the special reaction between SA and the biotin of HP2. As a result, the photocurrent direction of the electrode was switched from the anodic photocurrent to a cathodic photocurrent. Moreover, the cathodic photocurrent increased with the increase of miRNA-155 concentration. Based on this photocurrent-direction switching system and SDA strategy, miRNA-155 was detected sensitively (linear range, 0.1 fM - 10 nM; detection limit, 49 aM) with excellent selectivity due to the different photocurrent directions resulted from the target and interferents, and may have promising application in early tumor diagnosis by utilizing miRNAs as the biomarker.

The morphology and structure of CdSe QDs were investigated by transmission electron microscopy (TEM). It is noted that the average diameter of the CdSe QDs is about 5 nm (The inset plot in Fig. S1A, ESI†). From Fig. S1A, a lattice spacing of 0.348 nm, which corresponds to the (111) facet of CdSe QDs, can be observed. This implies the successful synthesis of CdSe QDs. On the other hand, CdSe QDs have a broad absorption region below about 550 nm (Fig. S1B, ESI†), implying that the as-prepared CdSe QDs should be a good photoactive material for the construction of a PEC biosensor.

The morphologies of ZIF-8, NPC-ZnO and AuNPs/NPC-ZnO polyhedra were investigated. As shown in Fig. S2A (ESI†), the ZIF-8 polyhedra have typical rhombic dodecahedron morphology with a uniform size of approximate 120 nm. After carbonization, NPC-ZnO polyhedra with uniform distribution of four elements (C, N, O and Zn) are prepared successfully (Figs. S2B and S2C, ESI†) and its average size is about 80 nm (Fig. S2D, ESI†), which is smaller than that of the ZIF-8 polyhedra. But, the morphology of NPC-ZnO polyhedra is similar with that of ZIF-8 polyhedra. For AuNPs/NPC-ZnO polyhedra (Fig. 1A), it is noted that Au NPs with an average size of about 5 nm are formed on the NPC-ZnO polyhedra. Furthermore, there are five elements (C, N, O, Zn and Au), which distribute uniformly on the AuNPs/NPC-ZnO polyhedra (Fig. 1B). These results indicate the successful deposition of AuNPs on the NPC-ZnO polyhedra.

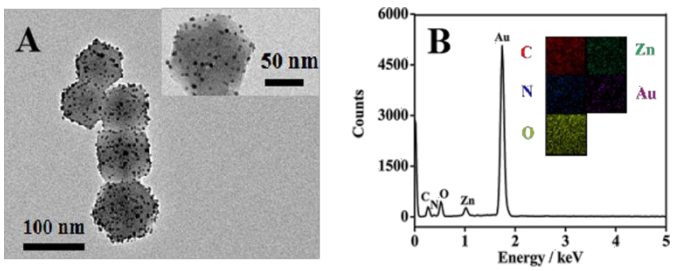

Fig. 1. TEM images (A) and EDX spectrum (B) of AuNPs/NPC-ZnO polyhedra. The inset in B is the corresponding elemental distribution.

The UV-vis absorption spectra of ZnO NPs, NPC-ZnO polyhedra and AuNPs/NPC-ZnO polyhedra are displayed in Fig. S2F (ESI†). ZnO NPs (about 130 nm in Fig. S2E, ESI†) exhibit a characteristic peak at 380 nm, which matches well with the band gap at 3.37 eV.[25] Compared to ZnO NPs, NPC-ZnO polyhedra display a wider light absorption edge that extends to the visible light range and the maximum absorption peak of NPC-ZnO polyhedra red-shifts to 418 nm, due to the interaction between NPC and ZnO.[26-28] For AuNPs/NPC-ZnO polyhedra, there is a very weak peak around 530 nm and the maximum absorption peak red-shifts to 436 nm, which is attributed to AuNPs on the NPC-ZnO polyhedra. The above results indicate that AuNPs/NPC-ZnO polyhedra have excellent light absorption properties in visible light range, which should be beneficial to the PEC bioassay.[29-31]

The developed PEC biosensor were characterized in detail. From Figs. S4-S6 (ESI†), it is noted that P-rGO (a thickness of about 0.87 nm, Fig. S3, ESI†) makes CdSe QDs be dispersed on the electrode surface uniformly and effectively enhances the photocurrent of CdSe QDs modified electrode. In Nyquist plot of electrochemical impedance spectroscopy (EIS) results, the semicircle diameter at higher frequencies corresponds to the electron transfer resistance (Rct) at the electrode. Compared to a small semicircle domain of the bare ITO electrode (curve a, Fig. 2A), the ITO/P-rGO electrode almost displays a straight line (curve b, Fig. 2A), suggesting the excellent electron transfer property of P-rGO. After modified with CdSe QDs, the Rct

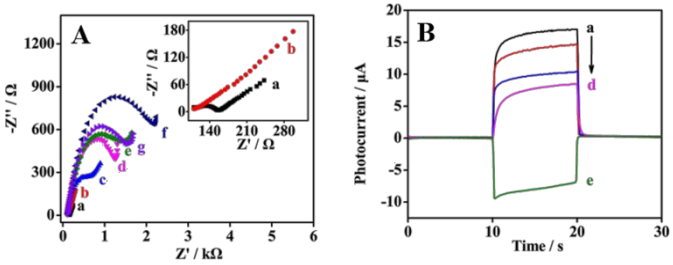

Fig. 2. (A) EIS in 0.1 M KCl solution containing 5 mM $K_3Fe(CN)_6/K_4Fe(CN)_6$ (1:1) in the frequency range from 0.01 Hz to 100 kHz at 5 mV. (a) bare ITO, (b) ITO/P-rGO, (c) ITO/P-rGO/CdSe QDs, (d) ITO/P-rGO/CdSe QDs/HP1, (e) ITO/P-rGO/CdSe QDs/HP1/MCH, (f) ITO/P-rGO/CdSe QDs/HP1/MCH/HP2, (g) ITO/P-rGO/CdSe QDs/HP1/MCH/HP2/SA-AuNPs/NPC-ZnO. (B) Photocurrent signals of the different electrodes in 0.1 M PBS (pH = 7.4) containing 0.1 M AA at -0.1 V. (a) ITO/P-rGO/CdSe QDs, (b) ITO/P-rGO/CdSe QDs/HP1, (c) ITO/P-rGO/CdSe QDs/HP1/MCH, (d) ITO/P-rGO/CdSe QDs/HP1/MCH/HP2, (e) ITO/P-rGO/CdSe QDs/HP1/MCH/HP2/AuNPs/SA-AuNPs/NPC-ZnO. The concentration of miRNA-155 is 100 pM.

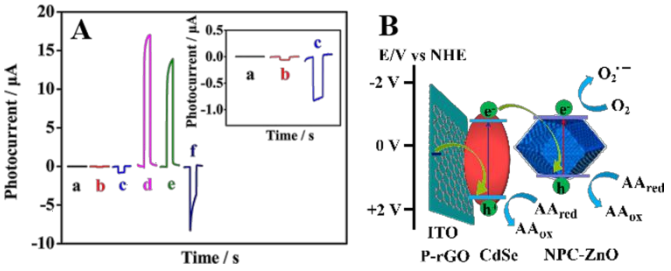

Fig. 3. (A) Photocurrent responses of ITO/ZnO (a), ITO/NPC-ZnO (b), , ITO/P-rGO/NPC-ZnO (c), ITO/P-rGO/CdSe QDs (d), ITO/P-rGO/CdSe QDs/ZnO (e) and ITO/P-rGO/CdSe QDs/NPC-ZnO (f) in 0.1 M PBS (pH = 7.4) containing 0.1 M AA at -0.1 V under visible light illumination. (B) The possible charge transfer process of the cathodic photocurrent generation at CdSe QDs//NPC-ZnO polyhedra system.

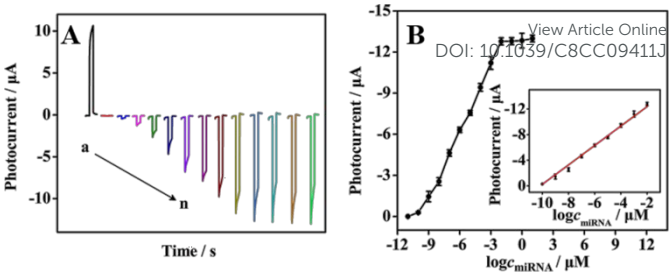

Fig. 4. (A) Photocurrent signals of the PEC biosensor to different concentrations of miRNA-155. From a to n: 0, 0.01 fM, 0.1 fM, 1 fM, 10 fM, 100 fM, 1 pM, 10 pM, 100 pM, 1 nM, 10 nM, 100 nM, 1 μM, 10 μM. (B) Dependence of photocurrents on the logarithm of miRNA-155 concentrations.

value of the electrode increases (curve c, Fig. 2A) because of the semiconductive features of CdSe QDs and the electrostatic repulsion action between MPA-capped CdSe QDs and $[Fe(CN)_6]^{3-/4-}$. After HP1, MCH, and HP2 are successively modified on the electrode, the Rct values successively increase (from curves d to f, Fig. 2A) due to the electrostatic repulsion between negatively charged HP1 (HP2) and anionic $[Fe(CN)_6]^{3-/4-}$, and blocking effect of MCH. But, the further modification of the SA-AuNPs/NPC-ZnO reduces the Rct value of the electrode (curve g, Fig. 2A) owing to the good conductive properties of SA-AuNPs/NPC-ZnO polyhedra. The results shown in Fig. 2A verify the successful construction of the PEC biosensor as displayed in Scheme 1.

The stepwise preparation process of the PEC biosensor was also monitored by PEC method. From Fig. 2B, it is noted that the ITO/P-rGO/CdSe QDs electrode has a large anodic photocurrent (curve a, 16.52 μA). When HP1, MCH, and HP2 are modified successively, the photocurrents of the electrode decrease gradually (curves b-d) due to the steric hindrance effects of these non-conductive molecules. However, after the introduction of SA-AuNPs/NPC-ZnO polyhedra to the electrode surface due to the specific interaction between SA on the SA-AuNPs/NPC-ZnO polyhedra and biotin on the biotin-labeled HP2, the switch of the photocurrent direction occurs and a large cathodic photocurrent can be observed (curve e, -9.546 μA). The above results reveal the potential possibility for miRNA-155 assay.

In order to explain the switch of photocurrent direction shown in Fig. 2B, several control experiments were carried out (Fig. 3A). The ITO/ZnO electrode generates hardly any photocurrent response (curve a). This should result from the fact that ZnO is beneficial to the absorption of UV light and the absorption efficiency for visible light (> 400 nm) is very low.[32] For NPC-ZnO polyhedra (curve b), a small cathodic photocurrent can be observed due to the red-shift of the absorption peak (Fig. S2F, ESI†). Furthermore, an enhanced cathodic photocurrent is obtained for the ITO/P-rGO/NPC-ZnO electrode (-0.832 μA, curve c), confirming the role of P-rGO on the improvement of the PEC performance of the electrode. When the ITO/P-rGO/CdSe QDs electrode is modified with ZnO NPs, the anodic photocurrent of the electrode decreases from 16.52 μA to 13.53 μA due to the steric hindrance effect of ZnO NPs (curves d and e). However, when the ITO/P-rGO/CdSe QDs electrode is modified with NPC-ZnO polyhedra, the photocurrent direction of the electrode is changed from the anodic current to cathodic current and a large cathodic current (-8.227 μA) is observed (curves d and f). These indicate clearly that the switch of the photocurrent direction shown in Fig. 2B results from the interaction between CdSe QDs and NPC-ZnO polyhedra. Noteworthy, the cathodic photocurrent of the ITO/P-rGO/CdSe QDs/NPC-ZnO polyhedra electrode is about 133 times larger than that of the ITO/NPC-ZnO polyhedra electrode.

To explore the possible charge transfer process for the cathodic photocurrent generation at CdSe QDs//NPC-ZnO Polyhedra system, the conduction band (CB) and the valence band (VB) of CdSe QDs and NPC-ZnO polyhedra were estimated by cyclic voltammetry (CV) (Fig. S7, ESI†).[33,34] The results display that CdSe QDs have a CB edge at -1.00 V and a VB edge at 1.41 V, and NPC-ZnO polyhedra have a CB edge at -1.06 V and a VB edge at 0.70 V vs saturated calomel electrode (SCE). That is, the CB and VB potentials of CdSe QDs are -0.76 and 1.65 V, and those of NPC-ZnO polyhedra are -0.82 and 0.94V vs the normal hydrogen electrode (NHE), respectively.

Based on the results shown in Fig. 3A and Fig. S7 (ESI†), a possible mechanism for the generation of cathodic photocurrent at CdSe QDs//NPC-ZnO Polyhedra system is displayed in Fig. 3B. Upon light excitation, the electrons and holes are produced from the CdSe QDs and NPC-ZnO polyhedra. Because the VB of NPC-ZnO polyhedra is lower than the energy level of ITO,[35] the photogenerated electrons of CdSe QDs easily transfer to the VB of NPC-ZnO polyhedra. On the other hand, the CB of NPC-ZnO polyhedra is more negative than the reduction potential of oxygen (-0.046 V vs NHE),[34] the dissolved O_2 molecules (electron acceptor) accept photogenerated electrons from NPC-ZnO polyhedra. Meanwhile, photogenerated holes oxidize AA_{red} to AA_{ox} and the recombination of photogenerated electron-hole pairs is reduced. Thus, a large cathodic photocurrent of the system is obtained.

Under the optimized experimental conditions (Fig. S8, ESI†), the analytical performance of the developed PEC biosensor for miRNA-155 assay were investigated. In the presence of miRNA-155, the photocurrent signal of the PEC biosensor is changed from the anodic photocurrent (background current) to cathodic photocurrent. And the cathodic photocurrent

increases with the increase of the miRNA-155 concentration (Fig. 4A). This implies that the developed PEC biosensor has excellent characteristics in avoiding false positive or negative signal, because the usual interferents (including redox active interferents and non-active interferents) just decrease or increase the anodic photocurrents of the PEC biosensor and can not switch the photocurrent direction of the electrode from anodic current to cathodic photocurrent.

Fig. 4B shows the dependence of photocurrent on the logarithm of miRNA-155 concentrations. A linear relationship can be observed in the range from 0.1 fM to 10 nM. The corresponding calibration equation is I (μA) = -1.516 logC_{miRNA} (μM) - 15.40 (R^2 = 0.9959), and a detection limit can be calculated to be 49 aM (3σ). The obtained detection limit is much lower than that reported previously (Table S2, ESI†). On the other hand, the developed PEC sensor exhibits excellent selectivity, good stability, acceptable reproducibility and satisfactory recovery in complex samples (Fig. S9, Table S3, ESI†).

In summary, a new photocurrent-direction switching system (CdSe QDs//NPC-ZnO polyhedra) has been developed in this work for PEC assay. Based on the matched energy level between CdSe QDs and NPC-ZnO polyhedra, a new PEC biosensor has been further developed by coupling CdSe QDs//NPC-ZnO polyhedra photocurrent-direction switching system with target-triggered SDA strategy, and miRNA-155 is detected sensitively (linear range, 0.1 fM-10 nM; detection limit, 49 aM). Furthermore, the PEC biosensor exhibited good stability and acceptable reproducibility. Importantly, the developed PEC platform has excellent selectivity due to the different photocurrent directions resulted from the target and interferents. The proposed photocurrent-direction switching system coupled with SDA strategy provides a new analytical platform for PEC assay and stimulates the exploitation of other photocurrent-direction switching systems to avoid false positive or negative signals as much as possible.

This work was financially supported by NSFC (21475035, 21727810), and the Foundation for Innovative Research Groups of NSFC (21521063).

Conflicts of interest

There are no conflicts of interest to declare.

Notes and references

1 N. Zhang, Y. F. Ruan, L. B. Zhang, W. W. Zhao, J. J. Xu, H. Y. Chen, *Anal. Chem.,* 2018, **90**, 2341−2347.
2 K. Yan, Y. Liu, Y. H. Yang, J. D. Zhang, *Anal. Chem.,* 2015, **87,** 12215−12220.
3 Z. L. Qiu, J. Shu, D. P. Tang, *Anal. Chem.,* 2018, **90,** 1021−1028.
4 M. J. Li, C. Xiong, Y. N. Zheng, W. B. Liang, R. Yuan, Y. Q. Chai, *Anal. Chem.,* 2018, ***90,*** 8211−8216.
5 F. E. Osterloh, *Chem. Soc. Rev.,* 2013, **42,** 2294−2320.
6 T. Hu, Y. N. Zheng, M. J. Li, W. B. Liang, Y. Q. Chai, R. Yuan, *Anal. Chem.,* 2018, **90,** 6096−6101.
7 X. H. Pang, Y. Zhang, J. H. Pan, Y. X. Zhao, Y. Chen, X. Ren, H. M. Ma, Q. Wei, B. Du, *Biosens. Bioelectron.,* 2016, **77,** 330−338.
8 Z. Y. Ma, Y. F. Ruan, F. Xu, W. W. Zhao, J. J. Xu, H. Y. Chen, *Anal. Chem.*, 2016, **88,** 3864−3871.
9 M. Zhao, G. C. Fan, J. J. Chen, J. J. Shi, J. J. Zhu, *Anal. Chem.,* 2015, **87,** 12340−12347.
10 W. W. Zhao, Z. Y. Ma, P. P. Yu, X. Y. Dong, J. J. Xu, H. Y. Chen, *Anal. Chem.,* 2012, **84,** 917−923.
11 Q. M. Shen, L. Han, G. C. Fan, J. R. Zhang, L. P. Jiang, J. J. Zhu, *Anal. Chem.,* 2015, **87,** 4949−4956.
12 B. Wang, J. T. Cao, Y. X. Dong, F. R. Liu, X. L. Fu, S. W. Ren, S. H. Ma, Y. M. Liu, *Chem. Commun.,* 2018, **54,** 806−809.
13 G. C. Fan, H. Zhu, D. Du, J. R. Zhang, J. J. Zhu, *Anal. Chem.,* 2016, **88,** 3392−3399.
14 E. H. Xiong, X. X. Yan, X. H. Zhang, Y. M. Li, R.Y. Yang, L.X. Meng, J. H. Chen, *Analyst,* 2018, **143,** 2799−2806.
15 R. Y. Yang, Y. M. Li, K. Zou, L. X. Meng, X. H. Zhang, J. H. Chen, *Chem. Commun.,* 2018, **54,** 4830−4833.
16 Q. Kang, Y. F. Chen, C. C. Li, Q. Y. Cai, S. Z .Yao, A. Grimes, *Chem. Commun.,* 2011, **47,** 12509−12511.
17 G. C. Fan, L. Z. Ma, S. Jayachandran, Z. M. Li, X. L. Luo, *Chem. Commun.,* 2018, **54,** 7062−7065.
18 C. X. Zhu, M.Y. Liu, X.Y. Li, X. H. Zhang, J. H. Chen, *Chem. Commun.,* 2018, **54,** 10359−10362.
19 M. J. Li, C. Xiong, Y. N. Zheng, W. B. Liang, R. Yuan, Y. Q. Chai, *Anal. Chem.,* 2018, **90,** 8211−8216.
20 L. S. Gong, H. D. Dai, S. P. Zhang, Y. Y. Lin, *Anal. Chem.,* 2016, **88,** 5775−5782.
21 C. G. Hu, J. O. Zheng, X. Y. Su, J. Wang, W. Z. Wu, S. S. Hu, *Anal. Chem.,* 2013, **85,** 10612−10619.
22 Q. Kang, L. X. Yang, Y. F. Chen, S. G. Luo, L. F. Wen, Q. Y. Cai, S. Z. Yao, *Anal. Chem.,* 2010, **82,** 9749−9754.
23 G. C. Fan, H. Zhu, D. Du, J. R. Zhang, J. J. Zhu, Y. H. Lin, *Anal. Chem.,* 2016, **88,** 3392−3399.
24 D. Jurkovicova, M. Magyerkova, L. Kulcsar, M. Krivjanska, V. Krivjansky, A. Gibadulinova, I. Oveckova, M. Chovanec, *Neoplasma,* 2014, **61,** 241−25.
25 S. M. Hatch, J. Briscoe, S. Dunn, *Adv. Mater.,* 2013, **25,** 867−871.
26 X. Zeng, L. Q. Huang, C. N. Wang, J. S. Wang, J. T Li, X. T. Luo, *ACS Appl. Mater. Interfaces,* 2016, **8,** 20274−20282.
27 R. Y. Yang, X. X. Yan, Y. M. Li, X. H. Zhang, J. H. Chen, *ACS Appl. Mater. Interfaces,* 2017, **9,** 42482−42491.
28 K. Shen, X. D. Chen, J. Y. Chen, Y. W. Li, *ACS Catal.,* 2016, **6,** 5887−5903.
29 Y. J. Li, M. J. Ma, J. J. Zhu, *Anal. Chem.,* 2012, **84,** 10492−10499.
30 D. Chen, H. Zhang, X. Li, J. H. Li, *Anal. Chem.,* 2010, **82,** 2253–2261.
31 Q. Kang, L. X. Yang, Y. F. Chen, S. L. Luo, L. F. Wen, Q. Y. Cai, S. Z. Yao, *Anal. Chem.,* 2010, **82,** 9749–9754.
32 R. S. Devan, R. A. Patil, J. H. Lin, Y. R. Ma, *Adv. Funct. Mater.,* 2012, **22,** 3326–3370.
33 G. L. Wang, J. X. Shu, Y. M. Dong, X. M. Wu, W. W. Zhao, J. J. Xu, H. Y. Chen, *Anal. Chem.,* 2015, **87,** 2892−2900.
34 L. Y.; Jin, Y. M. Dong, X. M. Wu, G. X. Cao, G. L. Wang, *Anal. Chem.,* 2015, **87,** 10429−10436.
35 X. M. Zhao, S. W. Zhou, L. P. Jiang, W. H. Hou, Q. M. Shen, J. J. Zhu, *Chem. Eur. J.,* 2012, **18,** 4974−4981.